Title

Molecular Structure of Copper and μ-Oxodiiron Octafluorocorrole Derivatives: Insights into Ligand Noninnocence

Journal

ACS Omega, 5(17)

ISSN

2470-1343

Authors

Thomas, Kolle E

Settineri, Nicholas S

Teat, Simon J

et al.

Publication Date

2020-05-05

DOI

10.1021/acsomega.0c01035

Peer reviewed

ACS OMEGA

http://pubs.acs.org/journal/acsodf

Article

Molecular Structure of Copper and μ-Oxodiiron Octafluorocorrole Derivatives: Insights into Ligand Noninnocence

Kolle E. Thomas, Nicholas S. Settineri, Simon J. Teat, Erik Steene, and Abhik Ghosh*

Cite This: *ACS Omega* 2020, 5, 10176−10182

Read Online

ACCESS | Metrics & More | Article Recommendations | Supporting Information

ABSTRACT: Single-crystal X-ray structures were obtained for the copper and μ-oxodiiron complexes of 2,3,7,8,12,13,17,18-octafluoro-5,10,15-triphenylcorrole, hereafter denoted as Cu[F_8TPC] and {Fe[F_8TPC]}$_2$O. A comparison with the crystal structures of other undecasubstituted Cu corroles, including those with H, Ar, Br, I, and CF_3 as β-substituents, showed that the degree of saddling increases in the order: H $\lesssim$ F < Ar $\lesssim$ Br $\lesssim$ I < CF_3. In other words, Cu[F_8TPC] is marginally more saddled than β-unsubstituted Cu triarylcorroles, but substantially less saddled than Cu undecaarylcorroles, β-octabromo-*meso*-triarylcorroles, and β-octaiodo-*meso*-triarylcorroles, and far less saddled than Cu β-octakis(trifluoromethyl)-*meso*-triarylcorroles. As for {Fe[F_8TPC]}$_2$O, the moderate quality of the structure did not allow us to draw firm conclusions in regard to bond length alternations in the corrole skeleton and hence also the question of ligand noninnocence. The Fe−O bond distances, 1.712(8) and 1.724(8), however, are essentially identical to those observed for {Fe[TPFPC]}$_2$O, where $TPFPC^{3-}$ is the trianion of 5,10,15-tris(pentafluorophenyl)corrole, suggesting that a partially noninnocent electronic structural description may be applicable for both compounds.

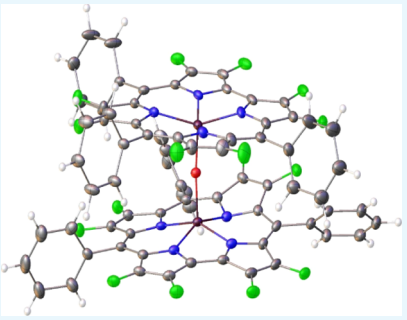

INTRODUCTION

Well over a half-century ago, the Danish chemist C. K. Jørgensen distinguished ligands as "innocent" and "suspect," a suspect—or "noninnocent," to use the modern term—ligand being one that leaves the oxidation state of the central metal uncertain or debatable.[1] In a typical situation, an electron or a hole cannot be approximated as belonging to either the metal or the ligand, but must be regarded as delocalized over the two.[2,3] Noninnocent ligands thus pose major challenges for inorganic spectroscopists and theoreticians.[4] Such ligands are also of considerable practical importance: by acting as reservoirs of electrons or holes, noninnocent ligands facilitate a variety of reactions that innocent ligands do not.[5] First-row transition metal corroles, as it happens, afford some of the best-characterized examples of noninnocent ligands.[6−9]

A variety of tools, spectroscopic and otherwise, have been used to characterize ligand noninnocence. Of these, NMR and EPR[10] spectroscopy are arguably the most direct because under favorable circumstances they provide a direct probe of the unpaired electron density. Paramagnetic FeCl and Fe−aryl corroles provide some of the most elegant examples of the use of ^{1}H NMR spectroscopy to elucidate the spin density distributions of noninnocent systems.[11−17] These methods, however, are useless for a considerable number of systems in which intramolecular spin couplings result in a diamagnetic ground state. Key examples of such cryptically noninnocent systems include copper,[18−21] μ-oxodiiron,[11,22] and iron−nitrosyl[23−25] corroles. For such systems, more indirect means, such as X-ray structure determination and electrochemistry, can be used to glean electronic structure information. It is against this backdrop that we report single-crystal X-ray structures of the copper and μ-oxodiiron complexes of 2,3,7,8,12,13,17,18-octafluoro-5,10,15-triphenylcorrole, hereafter denoted Cu[F_8TPC] and {Fe[F_8TPC]}$_2$O, respectively.

β-Octafluorinated porphyrins and corroles are uncommon ligands, primarily because of the relative inaccessibility of 3,4-difluoropyrrole.[14,26,27] However, they are of great interest because their metal complexes are expected to exhibit significantly perturbed reactivity as well as unusual solubility, conductivity, and optical properties. Thus, β-octafluorinated cobalt(III) corroles have been found to be highly active catalysts for water splitting, for both the oxygen[28] and hydrogen evolution reactions.[29] As strongly perturbed analogues of simple corroles, β-octafluorocorroles also afford fascinating subjects for studies of ligand noninnocence.[30] Such studies, however, have been hobbled by an almost[31] complete lack of X-ray crystal structures for β-octafluorocorrole derivatives, a gap in our knowledge that we have finally been able to close via this study.

Received: March 7, 2020
Accepted: April 10, 2020
Published: April 23, 2020

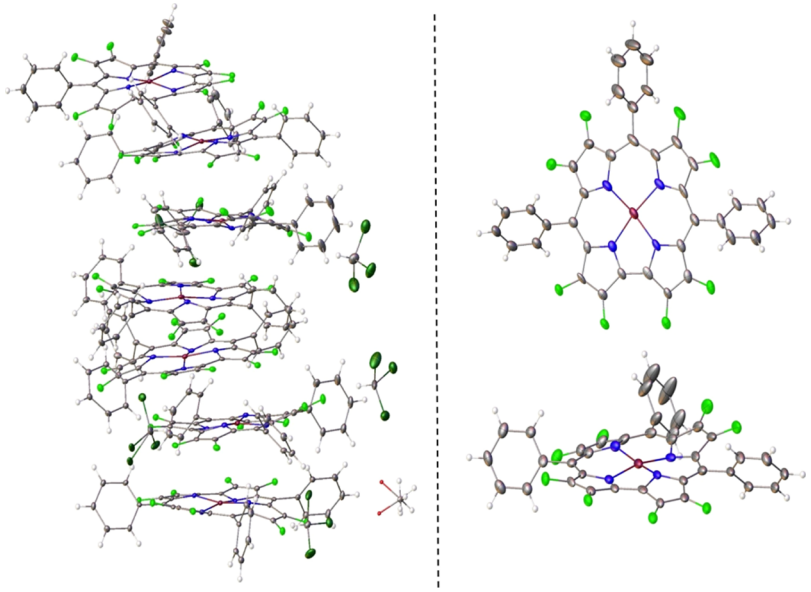

Figure 1. Thermal ellipsoid plots (at 30% probability) of Cu[F_8TPC]. Left: the seven Cu corroles in the asymmetric unit, along with solvent molecules ($CHCl_3$). Right: Close-up views of one of the Cu[F_8TPC] molecules.

RESULTS AND DISCUSSION

Ligand noninnocence manifests itself in copper corroles via a curious phenomenon that we have called intrinsic saddling.[32] Thus, copper corroles are saddled even in the absence of sterically hindering, peripheral substituents.[32,33] In the currently accepted picture, which is supported by an extensive array of structural, spectroscopic, electrochemical, and quantum chemical studies, saddling is engendered primarily by a Cu($d_{x^2-y^2}$)−corrole(π) orbital interaction, which endows the molecules with substantial Cu^{II}−$corrole^{\bullet 2-}$ character.[18−21,32−40] Sterically hindering substituents can accentuate the saddling,[34−40] but substituents alone, in the absence of the specific orbital interaction, do not bring about saddling in metallocorroles (the case of gold corroles being particularly instructive[41−46]). Interestingly, the corrolazine macrocycle, which has an even more contracted N_4 core than corroles and does not adopt noninnocent electronic structures as readily, yields planar, innocent Cu(III) complexes.[47] Likewise, carbacorroles such as azulicorrole also yield planar Cu(III) complexes.[48]

The X-ray structure of Cu[F_8TPC] (Figure 1, Tables 1 and 2) revealed distinctly saddled Cu−corrole macrocycles. Interestingly, a total of seven unique metallocorrole molecules were found in the asymmetric unit, providing significant insight into the plasticity of the macrocycle vis-à-vis saddling. Indeed, the saddling dihedrals defined and listed in Table 2 were found to vary over several degrees, as expected for a soft coordinate, and as for other Cu corrole derivatives, the following trend was observed: $\chi_1 < \chi_2 \approx \chi_3$. A comparison with crystal structures of other undecasubstituted Cu corroles, including those with H,[32,33] Ar,[35,36] Br,[20,34,37] I,[40] and CF_3[39] as β-substituents, proved instructive and showed that the degree of saddling increases in the order H $\lesssim$ F < Ar $\lesssim$ Br $\lesssim$ I < CF_3, which is essentially the order of their Charton[49] or Sterimol B1[50] steric parameters (Table 3).[51] In other words, Cu[F_8TPC] is marginally more saddled than β-unsubstituted Cu triarylcorroles, but substantially less saddled than Cu undecaarylcorroles, β-octabromo-*meso*-triarylcorroles, and β-octaiodo-*meso*-triarylcorroles, and far less saddled than Cu β-octakis(trifluoromethyl)-*meso*-triarylcorroles. It may be worth recalling that even for the exceptionally sterically hindered octakis(trifluoromethyl)-*meso*-triarylcorrole ligands, the Au

Table 1. Crystal and Refinement Data

	Cu[F_8TPC]	{Fe[F_8TPC]}$_2$O
empirical formula	$C_{37.86}H_{16.14}Cl_{2.14}CuF_8N_4O_{0.14}$	$C_{74}H_{30}F_{16}Fe_2N_8O$
formula mass	820.77	1462.76
temperature [K]	100(2)	100(2)
crystal system	monoclinic	monoclinic
space group	*P*21/*c*	*Cc*
λ [Å]	0.7288(1)	0.7288(1)
a [Å]	23.636(2)	20.065(3)
b [Å]	34.020(3)	21.913(3)
c [Å]	30.888(3)	16.255(3)
α [°]	90	90
β [°]	102.819(3)	98.773(5)
γ [°]	90	90
Z	28	4
V [Å]	24,218(3)	7063.4(19)
density [Mg m^{-3}]	1.576	1.376
crystal size (mm^3)	0.300 × 0.080 × 0.030	0.120 × 0.020 × 0.020
θ range [°]	1.183−21.498	2.106−22.654
meas. Reflections	384,508	51,140
unique reflections	25,642	8592
parameters	3358	911
restraints	36	38
R_{int}	0.0881	0.0647
R_1, wR_2 ($I > 2\sigma$)	0.0779, 0.2073	0.0669, 0.1728
R_1, wR_2 (all data)	0.0861, 0.2136	0.0696, 0.1774
S (GooF) all data	1.034	1.082
max/min res. dens. [e Å^{-3}]	1.406/−1.059	0.854/−0.396

https://dx.doi.org/10.1021/acsomega.0c01035
ACS Omega 2020, 5, 10176−10182

Table 2. Copper−Nitrogen Distances (Å) and Saddling Dihedrals (°) for the Seven Unique Molecules in the Asymmetric Unit of Cu[F_8TPC]

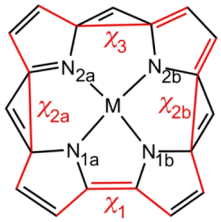

Cu[F_8TPC]	χ_1	χ_{2a}	χ_{2b}	χ_3	Cu−N_{1a}	Cu−N_{1b}	Cu−N_{2a}	Cu−N_{2b}
molecule 1	24.0(8)	44.7(1.5)	52.1(1.5)	52.9(1.3)	1.914(7)	1.902(7)	1.907(7)	1.909(7)
molecule 2	23.1(7)	49.0(1.2)	47.9(1.3)	56.1(1.2)	1.908(6)	1.915(7)	1.906(7)	1.904(6)
molecule 3	25.1(8)	49.8(1.5)	54.2(1.3)	62.1(1.4)	1.909(7)	1.907(7)	1.920(7)	1.908(8)
molecule 4	22.6(8)	50.8(1.5)	49.2(1.5)	52.5(1.3)	1.914(7)	1.905(8)	1.931(8)	1.904(7)
molecule 5	20.9(8)	47.7(1.5)	53.0(1.5)	54.9(1.3)	1.903(7)	1.899(7)	1.911(7)	1.903(8)
molecule 6	24.3(8)	49.4(1.6)	47.4(1.5)	48.8(1.4)	1.897(7)	1.910(8)	1.908(8)	1.920(7)
molecule 7	19.6(8)	44.3(1.4)	47.1(1.6)	49.3(1.3)	1.909(7)	1.896(7)	1.903(7)	1.904(7)

Table 3. Copper−Nitrogen Distances (Å) and Saddling Dihedrals (°) for Selected Cu Corroles

complex	Cu−N_1[a]	Cu−N_2[a]	χ_1	χ_2[a]	χ_3	refs
Cu[TPC]	1.891	1.891	27.5	53.4	48.7	33
Cu[F_8TPC]	1.897−1.914	1.896−1.915	19.6−24.3	44.3−54.2	48.8−62.1	this work
Cu[($p$$CF_3$Ph)$_8$TPC]	1.902	1.897	40.9	60.1	66.0	35
Cu[Br_8TpMePC]	1.916	1.916	44.7	65.9	57.3	20
Cu[I_8TpCNPC]	1.921	1.922	45.3	67.0	57.3	40
Cu[(CF_3)$_8$TpFPC]	1.921	1.925	57.2	86.4	84.5	39

[a]Average of two values for each experimental structure.

complex is rigorously planar because of the energetically mismatched nature of the Au($5d_{x^2-y^2}$)−corrole(π) orbital interaction.[46]

The X-ray structure of {Fe[F_8TPC]}$_2$O clearly revealed a linear Fe−O−Fe unit (Figures 2 and 3), as also observed for

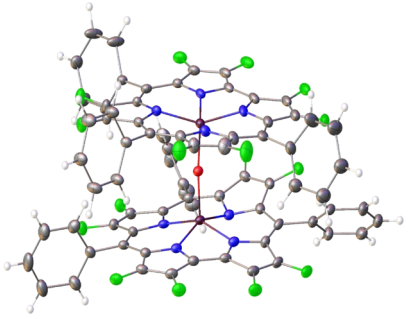

Figure 2. Thermal ellipsoid plots (at 30% probability) of {Fe[F_8TPC]}$_2$O.

{Fe[OEC]}$_2$O[52] and {Fe[TPFPC]}$_2$O,[53] where $TPFPC^{3-}$ is the trianion of 5,10,15-tris(pentafluorophenyl)corrole. Our earlier work has suggested that μ-oxodiiron corroles are noninnocent with a significant contribution with the following intramolecularly spin-coupled description[11,22]

$$\text{corrole}^{\bullet 2-}(\downarrow) - \text{Fe}^{\text{III}}(\uparrow\uparrow\uparrow) - \text{Fe}^{\text{III}}(\downarrow\downarrow\downarrow) - \text{corrole}^{\bullet 2-}(\uparrow)$$

One line of evidence in support of this conclusion is that the X-ray structure of {Fe[TPFPC]}$_2$O exhibits subtle but characteristic bond length alternations within and adjacent to the bipyrrole units of macrocycles, which are now recognized as a hallmark of noninnocent metallotriarylcorroles. Unfortunately, the moderate quality of the present structure (i.e., the e.s.d.'s in the corrole skeletal distances) does not allow us to draw a firm conclusion on this point. The Fe−O bond distances, 1.712(8) and 1.724(8), however, are essentially identical to those observed for {Fe[TPFPC]}$_2$O, which leads us to suggest that a partially noninnocent electronic structure description may also be apt for the present compound.

CONCLUSION

The X-ray structures of two β-octafluoro-*meso*-triphenylcorrole derivatives have afforded new insight into our growing understanding of the structural manifestations of ligand noninnocence in metallocorrole systems. Thus, Cu[F_8TPC] was found to be only slightly more saddled than β-unsubstituted Cu triarylcorroles and substantially less so than Cu β-octabromo-*meso*-triarylcorroles, consistent with the van der Waals radii of H, F, and Br. Accordingly, a noninnocent electronic structure, with substantial Cu^{II}−$corrole^{\bullet 2-}$ character, appears plausible for Cu[F_8TPC]. Unfortunately, the moderate quality of the X-ray structure of {Fe[F_8TPC]}$_2$O did not allow a definitive evaluation of ligand noninnocence based on an examination of the corrole skeletal bond distances. The fact that {Fe[F_8TPC]}$_2$O exhibits a nearly identical geometry for the Fe−O−Fe moiety as {Fe[TPFPC]}$_2$O, however, suggests that the two compounds probably share a similar, partially noninnocent electronic structure.

MATERIALS AND INSTRUMENTATION

All reagents and solvents were generally used as purchased. Ultraviolet−visible (UV−vis) spectra were recorded on an HP

https://dx.doi.org/10.1021/acsomega.0c01035
ACS Omega 2020, 5, 10176−10182

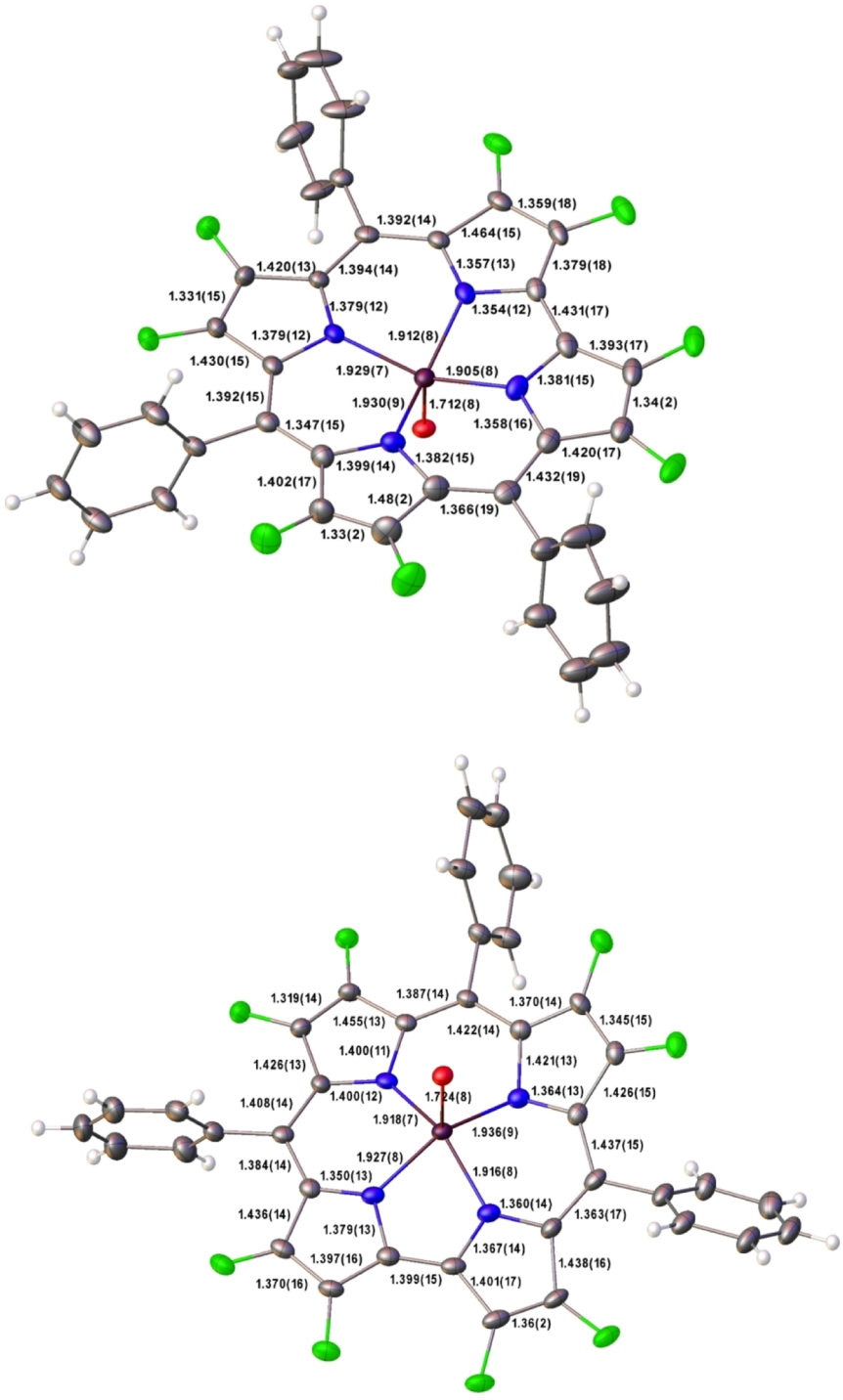

Figure 3. Selected crystallographic bond distances for $\{Fe[F_8TPC]\}_2O$.

8454 spectrophotometer. ^1H (400 MHz) and ^{19}F (376 MHz) NMR spectra were acquired on a 400 MHz Bruker AVANCE III HD spectrometer, equipped with a 5 mm BB/^1H (BB = ^{19}F, ^{31}P, and ^{15}N) SmartProbe in CD_2Cl_2 referenced to δ = 5.32 ppm and to 2,2,2-trifluoroethanol-d_3 (δ = −77.8 ppm), respectively. Mass spectra were recorded on an LTQ Orbitrap XL spectrometer. Free-base 2,3,7,8,12,13,17,18-octafluoro-5,10,15-triphenylcorrole, $H_3[F_8TPC]$, and $Cu[F_8TPC]$ were prepared as described previously.[14]

***μ*-Oxo-bis[2,3,7,8,12,13,17,18-octafluoro-5,10,15-triphenylcorrolatoiron], $\{Fe[F_8TPC]\}_2O$.** To a refluxing solution of $H_3[F_8TPC]$ (16 mg, 0.0239 mmol) in MeOH (8 mL) was added $FeCl_2{\cdot}4H_2O$ (24 mg, 0.121 mmol). After 0.5 h, when the Soret band of the free-base corrole was replaced by another at 378 nm, the reddish-brown mixture was allowed to cool and then evaporated to dryness. The residue was dissolved in CH_2Cl_2 (5 mL), to which was added 2 M aqueous NaOH (20 mL), and the resulting mixture was vigorously stirred for 45 min. The organic phase was then separated, gently washed with an equal volume of water, dried with anhydrous Na_2SO_4, and filtered. The filtrate was evaporated to dryness and dissolved in a minimum volume of $CHCl_3$. The resulting solution was chromatographed on a column of neutral alumina (activity I) with 1:1 *n*-hexane/

https://dx.doi.org/10.1021/acsomega.0c01035
ACS Omega 2020, 5, 10176−10182

CH_2Cl_2 as an eluent. The product was obtained as the first reddish-brown band. Yield: 7.0 mg (0.0048 mmol, 40%). Brown needles of X-ray quality were obtained by diffusion of *n*-hexane vapor into a concentrated solution of the compound in CH_2Cl_2 within 13 d.

UV−vis (CH_2Cl_2) λ_{max} [nm, $\varepsilon \times 10^{-4}$ (M^{-1} cm^{-1})]: 353 (Soret, 14.23). ^{1}H NMR: δ 7.62−7.54 (m, 4H), 7.54−7.44 (m, 10H), 7.44−7.37 (m, 8H), 7.25 (d, 4H, J = 7.40 Hz), 7.20 (t, 2H, J = 7.56 Hz), 6.71 (d, 2H, J = 7.32 Hz). ^{19}F NMR: δ −145.49 (s, 4F), −146.21 (d, 4F, J = 7.22 Hz), −147.80 (d, 4F, J = 7.41 Hz), −157.84 (s, 4F). MS (negative ion mode, major isotopomer) $[M]^-$: 1462.0936 (expt), 1462.0996 (calcd).

X-ray structure determination. X-ray data for Cu[F_8TPC] and {Fe[F_8TPC]}$_2$O were collected on the beamline 12.2.1 at the Advanced Light Source, Lawrence Berkeley National Laboratory. The crystals were mounted on a MiTeGen kapton loop and placed in a 100(2) K nitrogen cold stream provided by the Oxford Cryostream 800 Plus low-temperature apparatus on the goniometer head of a Bruker D8 diffractometer equipped with a PHOTON II CPAD detector operating in shutterless mode. Diffraction data were collected using synchrotron radiation monochromated using silicon (111) to a wavelength of 0.7288(1) Å. A full-sphere of data were collected for each crystal using a combination of phi and omega scans with scan speeds of 1.0 s per 4° for the phi scans and 1 s per degree for the omega scans at 2θ = 0 and −20, with different levels of beam attenuation, respectively. Absorption corrections were applied using SADABS.[54] The structures were solved by intrinsic phasing (SHELXT)[55] and refined by full-matrix least squares on F^2 (SHELXL-2014).[56] All nonhydrogen atoms were refined anisotropically. Hydrogen atoms were geometrically calculated and refined as riding atoms. For Cu[F_8TPC], definable solvent molecules were found in the electron density map as Q peaks and modeled appropriately; the peaks that could not be definitively assigned to either methanol or chloroform were treated with the solvent mask routine included in OLEX2.[57] Additionally, the crystal structure resolution was truncated at 0.99 Å because of resolution shells beyond 0.99 Å having R_{int} values greater than 25%. These additional higher resolution reflections have signal-to-noise ratios that are too low to contribute constructively to the structure solution and would have probably required additional restraints. For {Fe[F_8TPC]}$_2$O, the crystal structure resolution was truncated at 0.95 Å for the same reasons as indicated above for Cu[F_8TPC].

■ ASSOCIATED CONTENT

Supporting Information

The Supporting Information is available free of charge at https://pubs.acs.org/doi/10.1021/acsomega.0c01035.

^{1}H and ^{19}F NMR, mass, and UV−vis spectra (PDF)

Crystallographic data (CIF)

Crystallographic data (CIF)

Accession Codes

The crystal structures reported in this paper have been deposited at the Cambridge Crystallographic Data Centre and assigned the deposition numbers CCDC 1978931 and 1978935.

■ AUTHOR INFORMATION

Corresponding Author

Abhik Ghosh − *Department of Chemistry, UiT—The Arctic University of Norway, N-9037 Tromsø, Norway;* orcid.org/0000-0003-1161-6364; Email: abhik.ghosh@uit.no

Authors

Kolle E. Thomas − *Department of Chemistry, UiT—The Arctic University of Norway, N-9037 Tromsø, Norway*

Nicholas S. Settineri − *Advanced Light Source, Lawrence Berkeley National Laboratory, Berkeley, California 94720-8229, United States; Department of Chemistry, University of California Berkeley, Berkeley, California 94720, United States;* orcid.org/0000-0003-0272-454X

Simon J. Teat − *Advanced Light Source, Lawrence Berkeley National Laboratory, Berkeley, California 94720-8229, United States*

Erik Steene − *Department of Chemistry, UiT—The Arctic University of Norway, N-9037 Tromsø, Norway*

Complete contact information is available at: https://pubs.acs.org/10.1021/acsomega.0c01035

Notes

The authors declare no competing financial interest.

■ ACKNOWLEDGMENTS

This work was supported by NANO2021 grant no. 262229 of the Research Council of Norway (A.G.) and used resources of the Advanced Light Source, which is a DOE Office of Science User Facility under contract no. DE-AC02-05CH11231.

■ REFERENCES

(1) Jørgensen, C. K. Differences between the four halide ligands, and discussion remarks on trigonal-bipyramidal complexes, on oxidation states, and on diagonal elements of one-electron energy. *Coord. Chem. Rev.* **1966**, *1*, 164−178.

(2) Kaim, W.; Schwederski, B. Non-innocent ligands in bioinorganic chemistry - An overview. *Coord. Chem. Rev.* **2010**, *254*, 1580−1588.

(3) Eisenberg, R.; Gray, H. B. Noninnocence in Metal Complexes: A Dithiolene Dawn. *Inorg. Chem.* **2011**, *50*, 9741−9751.

(4) Ganguly, S.; Ghosh, A. Seven Clues to Ligand Noninnocence: The Metallocorrole Paradigm. *Acc. Chem. Res.* **2019**, *52*, 2003−2014.

(5) Lyaskovskyy, V.; de Bruin, B. Redox Non-Innocent Ligands: Versatile New Tools to Control Catalytic Reactions. *ACS Catal.* **2012**, *2*, 270−279.

(6) Ghosh, A.; Steene, E. High-Valent Transition Metal Centers and Noninnocent Ligands in Metalloporphyrins and Related Molecules: A Broad Overview Based on Quantum Chemical Calculations. *J. Biol. Inorg. Chem.* **2001**, *6*, 739−752.

(7) Thomas, K. E.; Alemayehu, A. B.; Conradie, J.; Beavers, C. M.; Ghosh, A. The Structural Chemistry of Metallocorroles: Combined X-ray Crystallography and Quantum Chemistry Studies Afford Unique Insights. *Acc. Chem. Res.* **2012**, *45*, 1203−1214.

(8) Ghosh, A. Electronic Structure of Corrole Derivatives: Insights from Molecular Structures, Spectroscopy, Electrochemistry, and Quantum Chemical Calculations. *Chem. Rev.* **2017**, *117*, 3798−3881.

(9) Nardis, S.; Mandoj, F.; Stefanelli, M.; Paolesse, R. Metal complexes of corrole. *Coord. Chem. Rev.* **2019**, *388*, 360−405.

(10) Krzystek, J.; Schnegg, A.; Aliabadi, A.; Holldack, K.; Stoian, S. A.; Ozarowski, A.; Hicks, S. D.; Abu-Omar, M. M.; Thomas, K. E.; Ghosh, A.; Caulfield, K. P.; Tonzetich, Z. J.; Telser, J. Advanced Paramagnetic Resonance Studies on Manganese and Iron Corroles with a Formal d^4 Electron Count. *Inorg. Chem.* **2020**, *59*, 1075−1090.

(11) Steene, E.; Wondimagegn, T.; Ghosh, A. Electrochemical and Electronic Absorption Spectroscopic Studies of Substituent Effects in

Iron(IV) and Manganese(IV) Corroles. Do the Compounds Feature High-Valent Metal Centers or Noninnocent Corrole Ligands? Implications for Peroxidase Compound I and II Intermediates. *J. Phys. Chem. B* **2001**, *105*, 11406−11413. ; Erratum: J. Phys. Chem.B 2002, 106, 5312

(12) Zakharieva, O.; Schünemann, V.; Gerdan, M.; Licoccia, S.; Cai, S.; Walker, F. A.; Trautwein, A. X. Is the Corrolate Macrocycle Innocent or Noninnocent? Magnetic Susceptibility, Mössbauer, ^{1}H NMR, and DFT Investigations of Chloro- and Phenyliron Corrolates. *J. Am. Chem. Soc.* **2002**, *124*, 6636−6648.

(13) Cai, S.; Licoccia, S.; D'Ottavi, C.; Paolesse, R.; Nardis, S.; Bulach, V.; Zimmer, B.; Shokhireva, T. K.; Walker, F. A. Chloroiron *meso*-Triphenylcorrolates: Electronic Ground State and Spin Delocalization. *Inorg. Chim. Acta* **2002**, *339*, 171−178.

(14) Steene, E.; Dey, A.; Ghosh, A. *β*-Octafluorocorroles. *J. Am. Chem. Soc.* **2003**, *125*, 16300−16309.

(15) Walker, F. A.; Licoccia, S.; Paolesse, R. Iron Corrolates: Unambiguous Chloroiron(III) (Corrolate)$^{2-\cdot}$ *π*-Cation Radicals. *J. Inorg. Biochem.* **2006**, *100*, 810−837.

(16) Ganguly, S.; Giles, L. J.; Thomas, K. E.; Sarangi, R.; Ghosh, A. Ligand Noninnocence in Iron Corroles: Insights from Optical and X-ray Absorption Spectroscopies and Electrochemical Redox Potentials. *Chem.—Eur. J.* **2017**, *23*, 15098−15106.

(17) Caulfield, K. P.; Conradie, J.; Arman, H. D.; Ghosh, A.; Tonzetich, Z. J. Iron(II) Corrole Anions. *Inorg. Chem.* **2019**, *58*, 15225−15235.

(18) Wasbotten, I. H.; Wondimagegn, T.; Ghosh, A. Electronic Absorption, Resonance Raman, and Electrochemical Studies of Planar and Saddled Copper(III) *meso*-Triarylcorroles. Highly Substituent-Sensitive Soret Bands as a Distinctive Feature of High-Valent Transition Metal Corroles. *J. Am. Chem. Soc.* **2002**, *124*, 8104−8116.

(19) Bröring, M.; Brégier, F.; Tejero, E. C.; Hell, C.; Holthausen, M. C. Revisiting the Electronic Ground State of Copper Corroles. *Angew. Chem., Int. Ed.* **2007**, *46*, 445−448.

(20) Thomas, K. E.; Vazquez-Lima, H.; Fang, Y.; Song, Y.; Gagnon, K. J.; Beavers, C. M.; Kadish, K. M.; Ghosh, A. Ligand Noninnocence in Coinage Metal Corroles: A Silver Knife-Edge. *Chem.—Eur. J.* **2015**, *21*, 16839−16847.

(21) Lim, H.; Thomas, K. E.; Hedman, B.; Hodgson, K. O.; Ghosh, A.; Solomon, E. I. X-ray Absorption Spectroscopy as a Probe of Ligand Noninnocence in Metallocorroles: The Case of Copper Corroles. *Inorg. Chem.* **2019**, *58*, 6722−6730.

(22) Ganguly, S.; Vazquez-Lima, H.; Ghosh, A. Wolves in Sheep's Clothing: *μ*-Oxo-Diiron Corroles Revisited. *Chem.—Eur. J.* **2016**, *22*, 10336−10340.

(23) Vazquez-Lima, H.; Norheim, H.-K.; Einrem, R. F.; Ghosh, A. Cryptic Noninnocence: FeNO Corroles in a New Light. *Dalton Trans.* **2015**, *44*, 10146−10151.

(24) Norheim, H.-K.; Capar, J.; Einrem, R. F.; Gagnon, K. J.; Beavers, C. M.; Vazquez-Lima, H.; Ghosh, A. Ligand noninnocence in FeNO corroles: insights from *β*-octabromocorrole complexes. *Dalton Trans.* **2016**, *45*, 681−689.

(25) Rahman, M. H.; Ryan, M. D.; Vazquez-Lima, H.; Alemayehu, A.; Ghosh, A. Infrared Spectroelectrochemistry of Iron-Nitrosyl Triarylcorroles. Implications for Ligand Noninnocence. *Inorg. Chem.* **2020**, *59*, 3232−3238.

(26) DiMagno, S. G.; Biffinger, J. C.; Sun, H. Fluorinated Porphyrins and Corroles: Synthesis, Electrochemistry, and Applications. In *Fluorine in Heterocyclic Chemistry*; Nenajdenko, V., Ed.; Springer: Cham, Switzerland, 2014; pp 589−620.

(27) Leroy, J.; Bondon, A. *β*-Fluorinated Porphyrins and Related Compounds: An Overview. *Eur. J. Org. Chem.* **2008**, 417−433.

(28) Dogutan, D. K.; McGuire, R., Jr.; Nocera, D. G. Electocatalytic Water Oxidation by Cobalt(III) Hangman *β*-Octafluoro Corroles. *J. Am. Chem. Soc.* **2011**, *133*, 9178−9180.

(29) Mahammed, A.; Mondal, B.; Rana, A.; Dey, A.; Gross, Z. The cobalt corrole catalyzed hydrogen evolution reaction: surprising electronic effects and characterization of key reaction intermediates. *Chem. Commun.* **2014**, *50*, 2725−2727.

(30) Liu, H.-Y.; Lai, T.-S.; Yeung, L.-L.; Chang, C. K. First Synthesis of Perfluorinated Corrole and Its MnO Complex. *Org. Lett.* **2003**, *5*, 617−620.

(31) Mondal, B.; Sengupta, K.; Rana, A.; Mahammed, A.; Botoshansky, M.; Dey, S. G.; Gross, Z.; Dey, A. Cobalt Corrole Catalyst for Efficient Hydrogen Evolution Reaction from H_2O under Ambient Conditions: Reactivity, Spectroscopy, and Density Functional Theory Calculations. *Inorg. Chem.* **2013**, *52*, 3381−3387.

(32) Alemayehu, A. B.; Gonzalez, E.; Hansen, L. K.; Ghosh, A. Copper Corroles Are Inherently Saddled. *Inorg. Chem.* **2009**, *48*, 7794−7799.

(33) Brückner, C.; Briñas, R. P.; Bauer, J. A. K. X-ray Structure and Variable Temperature NMR Spectra of [*meso*-Triarylcorrolato]-copper(III). *Inorg. Chem.* **2003**, *42*, 4495−4497.

(34) Alemayehu, A. B.; Hansen, L. K.; Ghosh, A. Nonplanar, Noninnocent, and Chiral: A Strongly Saddled Metallocorrole. *Inorg. Chem.* **2010**, *49*, 7608−7610.

(35) Berg, S.; Thomas, K. E.; Beavers, C. M.; Ghosh, A. Undecaphenylcorroles. *Inorg. Chem.* **2012**, *51*, 9911−9916.

(36) Gao, D.; Canard, G.; Giorgi, M.; Balaban, T. S. Synthesis and Characterization of Copper Undecaarylcorroles and the First Undecaarylcorrole Free Base. *Eur. J. Inorg. Chem.* **2012**, 5915−5920.

(37) Thomas, K. E.; McCormick, L. J.; Carrié, D.; Vazquez-Lima, H.; Simonneaux, G.; Ghosh, A. Halterman Corroles and Their Use as a Probe of the Conformational Dynamics of the Inherently Chiral Copper Corrole Chromophore. *Inorg. Chem.* **2018**, *57*, 4270−4276.

(38) Thomas, K. E.; Wasbotten, I. H.; Ghosh, A. Copper *β*-Octakis(trifluoromethyl)corroles: New Paradigms for Ligand Substituent Effects in Transition Metal Complexes. *Inorg. Chem.* **2008**, *47*, 10469−10478.

(39) Thomas, K. E.; Conradie, J.; Hansen, L. K.; Ghosh, A. A Metallocorrole with Orthogonal Pyrrole Rings. *Eur. J. Inorg. Chem.* **2011**, 1865−1870.

(40) Thomassen, I. K.; McCormick, L. J.; Ghosh, A. Synthesis and Molecular Structure of a Copper Octaiodocorrole. *ACS Omega* **2018**, *3*, 5106−5110.

(41) Because of the high energy of the Au($5d_{x^2-y^2}$) orbital, Au($5d_{x^2-y^2}$)-corrole(*π*) interactions do not lead to a noninnocent, saddled corrole.[42−46]

(42) Alemayehu, A. B.; Ghosh, A. Gold Corroles. *J. Porphyrins Phthalocyanines* **2011**, *15*, 106−110.

(43) Rabinovich, E.; Goldberg, I.; Gross, Z. Gold(I) and Gold(III) Corroles. *Chem.—Eur. J.* **2011**, *17*, 12294−12301.

(44) Thomas, K. E.; Alemayehu, A. B.; Conradie, J.; Beavers, C.; Ghosh, A. Synthesis and Molecular Structure of Gold Triarylcorroles. *Inorg. Chem.* **2011**, *50*, 12844−12851.

(45) Thomas, K. E.; Beavers, C. M.; Ghosh, A. Molecular Structure of a Gold *β*-Octakis(trifluoromethyl)-*meso*-triarylcorrole: An 85° Difference in Saddling Dihedral Relative to Copper. *Mol. Phys.* **2012**, *110*, 2439−2444.

(46) Thomas, K. E.; Gagnon, K. J.; McCormick, L. J.; Ghosh, A. Molecular structure of gold 2,3,7,8,12,13,17,18-octabromo-5,10,15-tris(4′-pentafluorosulfanylphenyl)corrole: Potential insights into the insolubility of gold octabromocorroles. *J. Porphyrins Phthalocyanines* **2018**, *22*, 596−601.

(47) Fox, J. P.; Ramdhanie, B.; Zareba, A. A.; Czernuszewicz, R. S.; Goldberg, D. P. Copper(III) and Vanadium(IV)−Oxo Corrolazines. *Inorg. Chem.* **2004**, *43*, 6600−6608.

(48) Larsen, S.; McCormick-McPherson, L. J.; Teat, S. J.; Ghosh, A. Azulicorrole. *ACS Omega* **2019**, *4*, 6737−6745.

(49) Charton, M. The Upsilon Steric Parameter—Definition and Determination. *Steric Effects in Drug Design*; Topics in Current Chemistry; Springer, 1983, Vol. *114*, pp 57−91.

(50) Verloop, A.; Hoogenstraaten, W.; Tipker, J. Development and Application of New Steric Substituent Parameters. In *Drug Design*; Ariens, E. J., Ed.; Academic Press: New York, 1976; Vol. *7*, pp 165−207.

(51) For a recent application of these parameters to an analysis of steric effects in dodecasubstituted porphyrins, see: Conradie, J.;

https://dx.doi.org/10.1021/acsomega.0c01035
ACS Omega 2020, 5, 10176−10182

Ghosh, A. Energetics of Saddling versus Ruffling in Metalloporphyrins: Unusual Ruffled Dodecasubstituted Porphyrins. *ACS Omega* **2017**, *2*, 6708−6714.
(52) Vogel, E.; Will, S.; Tilling, A. S.; Neumann, L.; Lex, J.; Bill, E.; Trautwein, A. X.; Wieghardt, K. Metallocorroles with Formally Tetravalent Iron. *Angew. Chem. Int. Ed. Engl.* **1994**, *33*, 731−735.
(53) Simkhovich, L.; Mahammed, A.; Goldberg, I.; Gross, Z. Synthesis and Characterization of Germanium, Tin, Phosphorus, Iron, and Rhodium Complexes of Tris(Pentafluorophenyl)Corrole, and the Utilization of the Iron and Rhodium Corroles as Cyclopropanation Catalysts. *Chem.—Eur. J.* **2001**, *7*, 1041−1055.
(54) Krause, L.; Herbst-Irmer, R.; Sheldrick, G. M.; Stalke, D. Comparison of silver and molybdenum microfocus X-ray sources for single-crystal structure determination. *J. Appl. Crystallogr.* **2015**, *48*, 3−10.
(55) Sheldrick, G. M. SHELXT- Integrated space-group and crystal-structure determination. *Acta Crystallogr., Sect. A: Found. Adv.* **2015**, *71*, 3−8.
(56) Sheldrick, G. M. Crystal structure refinement withSHELXL. *Acta Crystallogr., Sect. C: Struct. Chem.* **2015**, *71*, 3−8.
(57) Dolomanov, O. V.; Bourhis, L. J.; Gildea, R. J.; Howard, J. A. K.; Puschmann, H. OLEX2: a complete structure solution, refinement and analysis program. *J. Appl. Crystallogr.* **2009**, *42*, 339−341.

https://dx.doi.org/10.1021/acsomega.0c01035
ACS Omega 2020, 5, 10176−10182